HEFAT2012
9th International Conference on Heat Transfer, Fluid Mechanics and Thermodynamics
16 – 18 July 2012
Malta

CLOSURE TERM MODELING OF THE VOLUME AVERAGED TRANSPORT EQUATIONS FOR OPEN CELL FOAM

De Jaeger P.[1,2*], De Schampheleire S.[1], T'Joen C. [1], Huisseune H. [1], Ameel B. [1], De Paepe M. [1]
*Author for correspondence
[1] Department of Heat, Mass and Combustion Mechanics,
Sint-Pietersnieuwstraat 41, 9000 Gent, Belgium
[2] NV Bekaert SA, Bekaertstraat 2, 8550 Zwevegem, Belgium
E-mail: peter.dejaeger@ugent.be

ABSTRACT

A computational effective analysis method for the hydrodynamic phenomena which occur in foams, is possible by applying an up-scaling technique such as the volume-averaging method. This, however, results in additional terms which describe the influence of the microscopic transport phenomena on the macroscopic scale of analysis. Closure of the averaged equations is obtained by describing these terms as functions of averaged variables. In this paper, the closure modelling is done, based on first principles. The local viscous and pressure forces which act on the solid matrix are computed directly and related to classical porous properties, i.e., permeability and inertial factor. A flow regime dependency for the parameters is found and can be explained on physical grounds.

INTRODUCTION

Open-cell foams are hyper-porous materials, consisting of a fluid and a solid phase. In this paper, a single-phase fluid saturated foam is considered. Although the solid phase distribution in the foam domain is stochastic from nature, it possesses characteristic geometrical features. As such, non-overlapping sub-units are defined as cells. These cells are referred to as foam-cells, to distinguish them from the cells which define a computational domain. The solid material is found in the struts (or ligaments) which are positioned around the foam-cells. According to the Plateau rules, four struts have to meet in a node. This results in a single network, forming the solid phase. Characteristic for open-cell foams is the interconnection of foam-cells through pores. This allows a fluid to flow through the foam domain. The introduced terminology is illustrated in Figure 1.

NOMENCLATURE

A_0	[m²]	Strut cross-sectional surface area
A_{fs}	[m²]	Fluid-solid interfacial surface area
C	[-]	Cell Courant number ($C = {v\Delta t}/{\Delta x}$, with Δt the time step and Δx the size of the computational cell in flow direction
d	[m]	Diameter
I	[-]	Turbulent intensity
$\vec{\vec{I}}$	[-]	Identity tensor
k	[m²/s²]	Turbulent kinetic energy
l	[m]	Characteristic length ($l = \sqrt{{4A_0}/{\sqrt{3}}}$)
L	[m]	Linear dimension of the REV
$\vec{n}$	[-]	Normal vector on fluid-solid interface, pointing outward the fluid phase
P	[Pa]	Pressure
R_{uu}	[-]	Two-point correlation between streamwise velocity components
Re	[-]	Reynolds number ($Re = {\rho\|\langle\vec{v}\rangle\|l}/{\mu}$)
t	[s]	Time
u	[m/s]	Velocity component in x-direction
$\vec{v}$	[m/s]	Velocity vector
V	[m³]	Fluid phase volume in the REV
x	[m]	Cartesian axis direction
y	[m]	Cartesian axis direction
z	[m]	Cartesian axis direction

Special characters

β	[m⁻¹]	Inertial loss factor
σ_0	[m²/m³]	Surface-to-volume ratio
ϕ	[-]	Porosity
κ	[m²]	Permeability
ρ	[kg/m³]	Density
η	[m]	Kolmogorov scale
μ	[Pa.s]	Dynamic viscosity
ψ	[-]	Arbitrary quantity

Subscripts

i	Intrinsic average

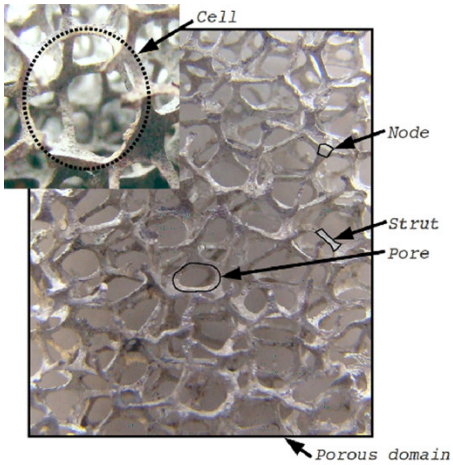

Figure 1 Foam terminology applied in this paper

Fluid flow through open-cell foams is of major importance for many applications [1]. Most widely used for its analysis is the Hazen-Dupuit-Darcy or Darcy-Forchheimer equation, given by:

$$\phi\nabla\langle P\rangle^i = \frac{\mu}{\kappa}\langle\vec{v}\rangle^i + \rho\beta\left\|\langle\vec{v}\rangle^i\right\|\langle\vec{v}\rangle^i, \qquad (1)$$

where $\langle P\rangle^i$ resembles the intrinsically averaged static pressure, $\langle\vec{v}\rangle^i$ the intrinsically averaged (or filtration) velocity, μ and ρ are respectively dynamic viscosity and fluid density and ϕ is porosity. The characteristics of the internal architecture of the solid phase are account for via κ and β, respectively known as permeability and inertial loss factor.

These two properties are considered to be material properties. They are typically obtained by considering one-dimensional flow. Interpolating a second-order polynomial through a dataset consisting of pressure drop versus Darcian (or superficial or seepage) velocity allows to readily derive both parameters. Note that this approach is applied on data which is obtained experimentally, as well as via computational fluid dynamics (CFD). This method, however, results in a large scatter in the data which is published in open-literature. Bonnet et al. [2] reviewed this, showing differences up to two decades. They contribute this to neglecting compressibility effects. Another source may be contributed on the amount of data which serves for interpolation, as indicated by Innocentini et al. [3]. On more physical grounds, variations in the flow parameters have also been contributed to the walls confining the foam domain [4], the existence of entrance/exit effects [5] and dependency on the flow regime [6].

A more theoretically analysis of flow phenomena in open-cell foam can be obtained by upscaling the flow equations from the continuum-scale (or microscopic-scale) to the natural-scale (or macroscopic-scale) of foam. Microscopic-scale refers to the scale at which the Navier-Stokes equations are valid (i.e., sufficiently low Knudsen number such that molecular-scaled phenomena become irrelevant). The macroscopic-scale is a linear dimension of a representative elementary volume (REV) as defined by Bear [7]. Following Cushman et al. [8], the existence of the macroscopic-scale makes open-cell foam a discrete hierarchical material, which indicates that there exists a clear-cut length scale separation between the micro- and macroscopically scaled physics. Remark though, that this implies that the averaged depending variables over a REV have to behave quasi-steady, compared to their continuum-scaled counterparts.

The length-scale separation makes it convenient to perform the upscaling via the volume-averaging theory, as described by Whitaker [9]. The resulting flow equations for incompressible flow with constant fluid properties in the REV, stationary solid phase and constant porosity are then given by:

$$\nabla.\langle\vec{v}\rangle = 0 \qquad (2)$$

$$\rho\frac{\partial\langle\vec{v}\rangle}{\partial t} + \rho\nabla.\left(\frac{\langle\vec{v}\rangle\langle\vec{v}\rangle}{\phi}\right) = -\phi\nabla\langle P\rangle^i + \mu\nabla^2\langle\vec{v}\rangle$$
$$-\rho\nabla.\langle\tilde{\vec{v}}\tilde{\vec{v}}\rangle + \frac{1}{V}\iint_{A_{fs}}\vec{n}_{fs}.\left(-\tilde{P}\vec{I} + \mu\nabla\tilde{\vec{v}}\right)dA \qquad (3)$$

For both terms on l.h.s. and the first two terms on the r.h.s. of equation (3), the depending variables are evaluated on the macroscopic scale. The latter two terms on the r.h.s. take the local spatial deviations in account, which for an arbitrary quantity ψ result from a spatial decomposition given by: $\psi = \langle\psi\rangle^i + \tilde{\psi}$ [10]. These terms act as source terms in the evaluation of the macroscopic-scaled depending variables and express the influence of the microscopic physics on the macroscopic scale of analysis. Note that equation (3) takes the form of the Navier-Stokes equation, allowing to use known solution methods. This, however, requires that the integral term is related to macroscopic quantities, which defines the closure problem.

The first source term describes momentum dispersion. Inspired by Large Eddy Simulation (LES) turbulence modelling, a constitutive relation contributes the small-scaled motions to the diffusion of the macroscopic-scaled momentum, when there is a strain field on this scale. Note that these motions are triggered by the presence of the solid matrix and not by the mechanisms which trigger turbulence. Hence, effective viscosity has a different meaning than the eddy-viscosity in turbulence modelling. To implement this closure model, it suffices to replace the fluid viscosity in second term on the r.h.s. of equation (3) with the summation of the fluid and effective viscosity (because they do not mutually correlate).

The second source term on the r.h.s. of equation (3) results from the no-penetration and no-slip boundary conditions near the solid-fluid interface and results in a pressure drag and viscous drag force. V resembles the total volume of the REV in this term, $\vec{n}_{fs}$ is the normal vector on the fluid-solid interface and A_{fs} is the fluid-solid interfacial surface. For a macroscopically steady and fully developed flow (thus no entrance/exit effects or influences of no-slip or free-flow boundaries of the foam domain) and after implementing the momentum dispersion closure model, equation (3) reduces to:

$$\phi\nabla\langle P\rangle^i = \frac{1}{V}\iint_{A_{fs}}\vec{n}_{fs}.\left(-\tilde{P}\vec{I} + \mu\nabla\tilde{\vec{v}}\right)dA \qquad (4)$$

Whitaker [11] showed theoretically that closing this equation results in the Darcy-Forchheimer equation (1). Therefore, the permeability and inertial loss factor (in tensorial form) are given by:

$$\overleftrightarrow{\kappa} = \mu\langle\vec{v}\rangle^i V\left[\iint_{A_{fs}} \vec{n}_{fs}.\left(\mu\nabla\tilde{\vec{v}}\right)dA\right]^{-1} \quad (5)$$

$$\overleftrightarrow{\beta} = -\frac{\left(\langle\vec{v}\rangle^i\right)^{-1}}{\rho\|\langle\vec{v}\rangle^i\|V}\left[\iint_{A_{fs}} \vec{n}_{fs}.\left(\tilde{P}\overleftrightarrow{I}\right)dA\right] \quad (6)$$

Recognizing that the integrals in these equations are respectively the viscous and the pressure force which act on the fluid-solid interface gives a physical interpretation to both parameters.

To the best knowledge of the authors, these forces have not been computed directly, which motivates the present work.

SIMULATION PROCEDURE

The goal is to solve numerically for both forces, for flow regimes ranging from creeping to turbulent. This is done using the commercial solver Ansys®. This requires a geometrical model which is representative for the foam's internal architecture. The most accurate model available is a virtual reproduction via a micro-computed tomography (μCT) scan. The resulting REV consists of at least two foam-cells in each direction [12], containing 8 foam-cells in total. Recalling the fully-developed flow assumption, periodicity in the three directions has to be applied. This is not the case for a μCT-based model, restricting its applicability for solving equations (5) and (6).

A second issue is the required grid quality to resolve the viscous boundary layer near the fluid-solid interface, in order to obtain a sufficiently accurate numerical approximation of the wall shear stress in equation (5). Furthermore, the complexity of the geometry results in an unstructured grid, making a first order approximation of the normal velocity gradient only sufficiently accurate when the cells adjacent to the fluid-solid interface are small enough. A proper estimation of the required distance from the adjacent cell centroid (y_c) to the solid-fluid interface is given by (see the Fluent manual for more details):

$$y_c\sqrt{\frac{\rho\langle\vec{v}\rangle}{\mu x_0}} \leq 1, \quad (7)$$

where x_0 is the distance in flow direction, along the fluid-solid interface. For a Darcian velocity of 10 m/s and x_0 chosen at 0.05 of a characteristic measure of the strut thickness (i.e. solve 95% of the viscous boundary layer), results in $y_c \approx 8\ \mu$m (for ρ = 1 kg/m³ and μ = 1.79x10^{-5} Pa.s). The cells from the fluid-solid interface are allowed to grow in the fluid phase. The growth rate needs to be limited (a factor 1.1 is used in this paper), as it influences the gradient approximation in the numerical scheme. The result is that in a μCT-based REV, the number of cells would be in the order of 1x10^8. This is found practically insolvable with the available commercial solver.

A solution is found by using the μCT data of the studied foam to quantify the characteristic geometrical features. This is done by determining the averaged values from a foam volume containing approximately 30 foam-cells. The results are obtained from De Jaeger et al. [13] and reproduced in table 1 for the studied geometry. d_1 and d_2 are respectively the small and large diameters of the ellipsoid encompassing an average foam-cell, A_0 is the cross-sectional surface area and σ_0 is the surface-to-volume ratio.

d_1 [mm]	d_2 [mm]	A_0 [10^{-1} mm²]	ϕ [-]	σ_0 [m^{-1}]
4.22	6.23	0.998	0.932	440

Table 1 Characteristic geometrical dimensions

Following De Jaeger et al. [13], a periodic unit foam-cell (PUC) can be generated via a journal file in the pre-processor Gambit®. The resulting PUC geometry is shown in figure 2(a). Note that the strut geometry is based on two empirical correlation which account for the strut cross-sectional shape and surface area variation between two nodes.

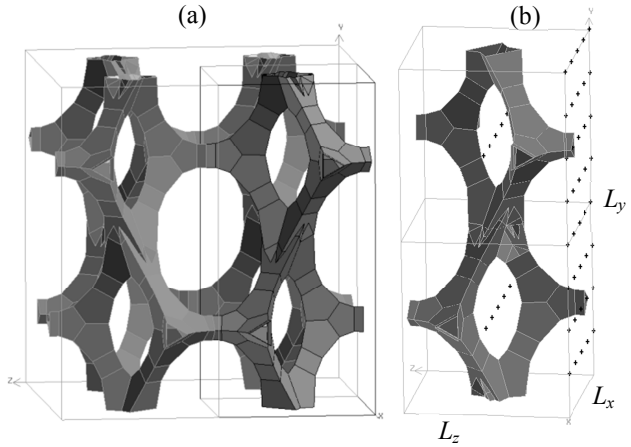

Figure 2 (a) Foam periodic unit cell, (b) computational domain with the locations where local velocity is monitored

A more detailed study of the PUC reveals that a sub-volume bares additional periodicity, as is depicted in figure 2(b). The dimensions are $L_x = L_z$ = 3.03 mm and L_y = 6.42 mm. In this case, the lower half of the boundary plane at x = 0 is periodic with the upper half of the boundary plane at $x = L_x$. The same holds for the upper half at x = 0 versus the lower half at $x = L_x$. The same periodicity can be retrieved in the z-direction. A classical periodic boundary condition is applied in the y-direction, resulting in a fully periodic flow domain as is required for equations (5) and (6) to be valid. The size of the flow domain, however, must still be large enough to ensure that all microscopically scaled physics. Therefore, the dimensions in all three directions should be at least twice the size of the largest eddies (or integral length scale) [14].

The flow regimes are characterised in this paper by a Reynolds number based on the Darcian velocity and the side of an equilateral triangle with surface area A_0, as characteristic length l (which is 0.48 mm for the foam in this paper). For the earlier mentioned velocity and fluid properties, Re = 268, Hutter et al. [15] performed simultaneously particle image

velocimetry (PIV) and laser induced fluorescene LIF measurements, for Re ranging from 27 to 337. For Re = 202 and their highest Reynolds number flow, their turbulent intensity is nearly constant (I = 0.23). The authors concluded that the flow can be considered turbulent. It should be noted though, that a comparison with the flow regimes behind a triangular cylinder suggests that the flow regime studied here will be in the transitional regime rather than fully turbulent [16]. A velocity field visualisation by Onstad et Al. [17] revealed that the flow field contains coherent jet structures which pass through pores. In the core of these jets, velocity gradients can be expected to be considerable less than near the solid-fluid interface. Based on these observations and to keep the computational cost affordable, the largest cell size is taken 5 times larger than the Kolmogorov scale. Therefore, the simulation done on the fine grid cannot be guaranteed to be a fully resolved DNS; rather it has to be seen as an implicit LES.

The Kolmogorov scale (η) is an estimate of the smallest length-scales in highly turbulent flow regimes. Following Pope [18], η depends on the turbulent kinetic energy (k), which is readily available from the turbulent intensity. The corresponding turbulent Reynolds number (Re_t) can be calculated, resulting in a measure for the Kolmogorov scale via following relations:

$$k = {}^3/_2\,(\overline{\|\langle\vec{v}\rangle\|I})^2 \qquad Re_t = \frac{\rho\sqrt{k}l}{\mu} \qquad \frac{l}{\eta} = {Re_t}^{3/4}$$

Based on the previous reasoning, the largest cell size is set at 100 µm. The final cell sizes for the finest grid thus grow from a size of 8µm to a largest size of 100µm with growth rate 1.1.

For the other two grids, these cell sizes are doubled. The resulting skewness and cell count is given in table 2. The second to last column gives the percentage of the cell count with skewness larger than 0.5. This can be seen as the limit between a good (skewness < 0.5) and acceptable (0.5 < skewness < 0.8) mesh, as can be read from the Gambit® manual. The equiangle skewness is reported as this yielded for all three grids the highest value, compared with equisize skewness.

The equations to be solved are the incompressible Navier-Stokes equations. The diffusive term is discretised via a second-order central differencing scheme. For the finest grid, the convective term is discretised via a second-order accurate central-differencing scheme. For the other two grids, the bounded central differencing is used for the convective term (which is a blending between second-order central differencing and upwind, depending on the cell Reynolds number). Implicit dual time-stepping is used as unsteady formulation. In case of unsteady simulations (Re>28), the time step is chosen to ensure that the cell based Courant numbers are less than 1. The first 10 flow through cycles are discarded to ensure that unphysical fluctuations have vanished. The final data is captured from three subsequent flow through cycles.

Because the grids are unstructured, the gradients are evaluated via the least-squares method. Solutions are obtained via the pressure-based coupled solver, with double-precision accuracy. Convergence in all computations reached 10^{-6} for continuity and 10^{-8} for the velocity components, within 20 iterations per time step.

Grid	Min cell	Max cell	Max skew	Skew > 0.5	Total cell count
Fine	8 µm	100 µm	0.83	8.3%	30621891
Mid	16 µm	200 µm	0.83	8.2%	8282347
Coarse	32 µm	400 µm	0.82	8.1%	2285731

Table 2 Minimum- and maximum cell size of the three grids, as well as the maximum skewness, the part of the grid with skewness > 0.5 and the total cell count.

Grid	y^+ [-]	C [-]	R [-]	$\langle u\rangle^i$ [m/s]	κ_{xx} [10^{-7}m²]	β_{xx} [m^{-1}]
Fine	0.23	0.16	23.1	9.99	8.06	194.38
Mid	0.42	0.16	26.3	9.96	7.91	194.16
Coarse	0.78	0.3	30.4	9.87	7.78	194.05

Table 3 Averaged wall y^+, cell Courant (C) and Reynolds (R) number. The x-component of the intrinsically averaged velocity and first components of the permeability and inertial factor is given, for the three grids.

RESULTS

Up to 390000 iterations are performed on the three grids. This is done on two machines, equipped with dual hex core Xeon X5690 3.46GHz processors with 12MB cache. The on-board memory is respectively 48 and 96 GB DDR3-1333MHz RAM. The operating system is Scientific Linux 5.5, 64-bit. The computation of the finest grid took 235 days, while the coarse grid finished within 12 days.

Grid independency

The grid independence is done for a pressure gradient of 20000 Pa/m in x-direction. Based on the geometrical characteristics of the foam, the permeability and inertial factor can be estimated from data in open literature [2]. The resulting intrinsic velocity is estimated to be 10 m/s. The mean wall y^+ values near the fluid-solid interface are given for the three grids in table 3, as well as the averaged cell Reynolds and Courant number. The latter is considerable smaller than 1 which favours accuracy. The intrinsically averaged velocity between the coarsest and finest grid only differs 1.2%, while the permeability and inertial factors respectively deviate 3.5% and 0.2%. This indicates that a grid independent solution is obtained for the relevant macroscopic variables.

A more thorough evaluation of the grid quality is based on the two-point correlation between streamwise velocities (u) at different streamwise (x-coordinate) locations but the same lateral (y-coordinate) and spanwise (z-coordinate) location. This is based on the local velocity monitoring, as depicted in figure 2(b). Ten correlation coefficients are obtained between the 10 points at x=0 and respectively at following dimensionless locations: x/L_x=0, 0.25, 0.5, 0.75 or 1. Averaging over these points yields R_{uu}, given by:

$$R_{uu} = \langle \frac{\overline{u(0,y,z,t)u(x,y,z,t)}}{\sqrt{\overline{u^2(0,y,z,t)}\;\overline{u^2(x,y,z,t)}}} \rangle \,, \qquad (8)$$

where the over-bar represents time-averaging and $\langle \cdots \rangle$ gives the spatial averaging of the ten local values. The result for the three grids is depicted in figure 3.

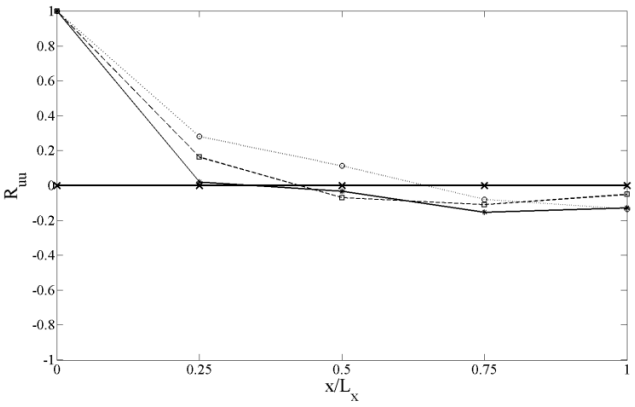

Figure 3 Zero-time-lag two-point correlation with streamwise separation of the streamwise velocity. -+-: fine mesh, -□-: mid mesh, ·Θ·: coarse mesh.

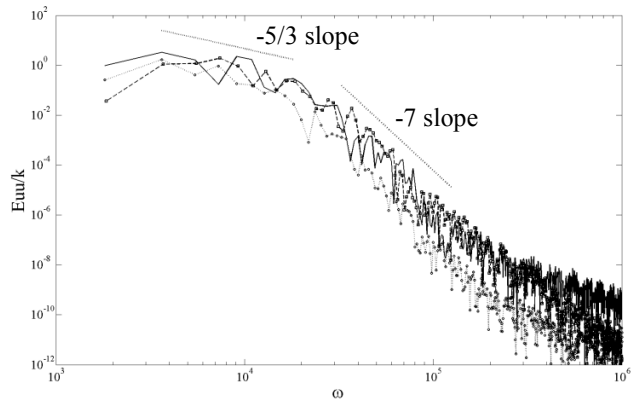

Figure 4 Turbulent spectrum of the normalized turbulent kinetic energy of the streamwise velocity component u, at location $x/L_x = 0.5$, $y/L_y = 0.5$, $z = 0$. Caption: see figure 3.

The point where the correlation becomes zero gives a measure for the integral length scale [19]. For the finest grid, this is obtained at a quarter of L_x. Comparing this with l, which is 0.16 when made dimensionless, and recognizing that the point where the correlation coefficient R_{uu} becomes zero is not accurately captured (due to a poor sampling of the streamwise separation and using only 10 points in a plane) suggests that l is an adequate characteristic length. The coarser grids clearly suggests a larger characteristic length for the large eddies. This can be contributed to numerical diffusion and additional diffusion stemming from the LES subgrid model.

Another, but less sensitive manner of examining grid convergence is comparing the power density spectra in different points. The spectrum of one point is depicted in figure 4. It clearly shows a relatively compact inertial subrange (-5/3 slope), followed by the viscous dissipation range (-7 slope). The latter seems to depend on the used grid. The finest grid shows the least dissipation in the higher frequency (ω) range, while the opposite is observed for the coarsest grid.

Reconstructing the applied pressure gradient of 20000 Pa/m results in 19755 Pa/m, 19517 Pa/m and 19152 Pa/m for respectively the fine, mid and coarse grid. The latter results in a deviation of 4.2%. Taking a compromise between accuracy and computational cost, the viscous boundary layer is solved with the 8µm cells, while the largest possible cell in the computational domain is set at 200µm. For all results presented in the remainder of this paper, this yields a maximum uncertainty of 1.2%. This clearly shows that the discussed method, based on first principles, allows to determine flow properties accurately.

Note that, although Figure 4 indicates that turbulence is triggered, the derived viscous and pressure forces allow to reconstruct the pressure drop with great accuracy. This is also observed for a simulation at higher Reynolds number (Re=370, resulting from 50kPa/m pressure gradient). This indicates that influences of turbulence on pressure drop are fully captured via the Darcy-Forchheimer equation and makes the usage of turbulent viscosities questionable; at least for the Reynolds numbers studied here.

Permeability

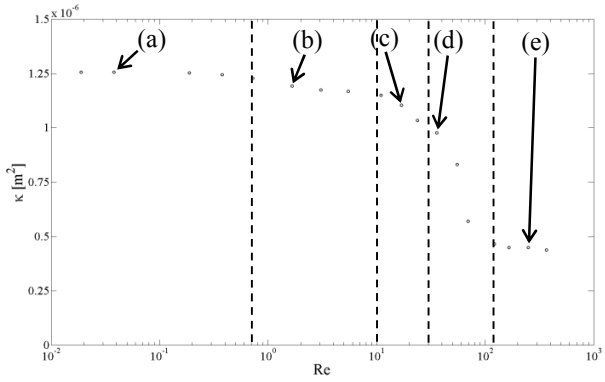

Figure 5 Permeability versus Reynolds number. Five flow regimes can be distinguished. The arrows indicate the points for which the flow pattern is depicted in Figure 6.

The permeability is determined by applying different pressure gradients in x-direction, ranging from 0.05 Pa/m to 50kPa/m. The corresponding Reynolds number varies between 0.019 and 370. The result is depicted in Figure 5. It clearly shows a significant dependency on the flow regime. Based on experimental data, Dukhan et al. [6] already reported this behaviour. Their 10PPI data is applicable for the foam structure used to study the flow properties. They analysed pressure drop versus velocity, which ranged from 0.5 to 20 m/s

(corresponding with Re ranging between 11 and 444). They considered their first two points (0.5 and 1 m/s) to be in the Darcy regime, while the flow regime with velocities above 5 m/s (i.e. Re=111) was referred to as the Forchheimer regime. Between 1 and 5 m/s, they considered the flow to be transitional. The permeability in the Darcy and Forchheimer regime was 1.01×10^{-4} and 4.29×10^{-7} m² respectively.

The numerical results confirm a quasi-constant permeability for Re>115. The corresponding permeability in this flow regime is 4.43×10^{-7}, which is in close agreement with the value that Dukhan et al. [6] found. For the lowest Reynolds numbers though, the found permeability is 1.255×10^{-6}, which significantly deviates from the data obtained by Dukhan et al. [6]. The difference can be contributed to two factors. First, Dukhan et al. [6] indicate that only two points are used for the the Darcy flow regime and that they are relatively at the high end of it. Secondly, Dukhan et al. [6] assumed a Darcy regime by neglecting the second term in equation (1). As will be demonstrated later, this assumption is not valid when the definitions given by equations (5) and (6) are used for permeability and inertial loss factor.

The numerical simulations allow to investigate the typical flow pattern for each flow regimes. These are depicted in Figure 6. In the first three flow regimes, the flow is laminar and steady. For the lowest Reynolds number, regime (a), an inertial core starts to form in the pores. The core does not span the complete flow domain and therefore has no influence on the struts downstream. This changes for the second flow regime, where the inertial core now spans the complete flow region. The permeability shows a slight decrease, as can be noted from Figure 5. Recalling equation (5), this implies that the strain rate (and thus shear stress for a Newtonian fluid) increases more than the filtration velocity increases, i.e., the effect of the inertial core formation is felt downstream in the foam.

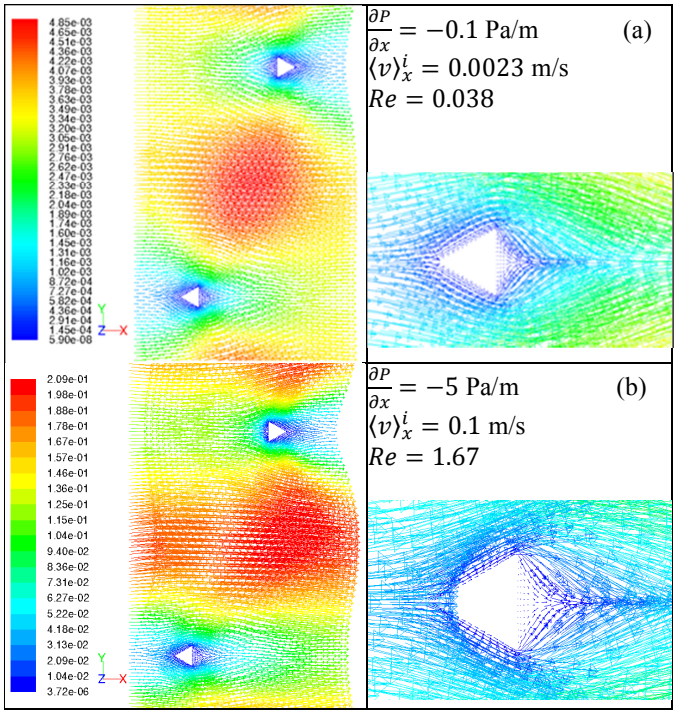

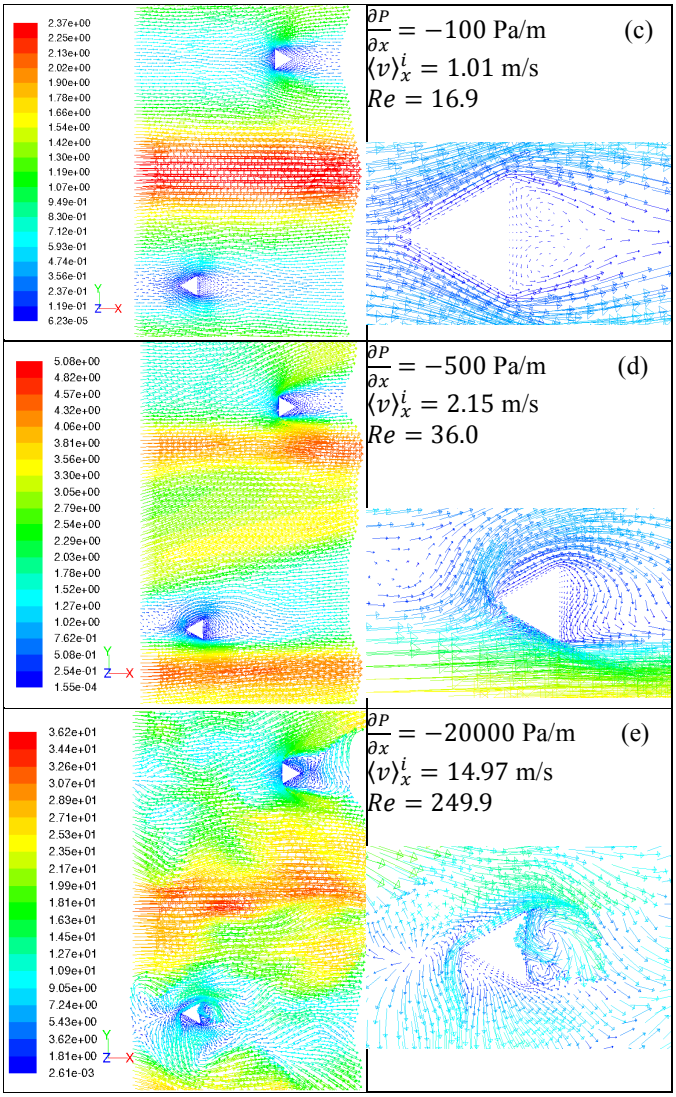

Figure 6 Typical flow patterns for the various flow regimes. For each case, a global view is show, together with a detail of the flow around the lower strut. Also given is the applied pressure gradient, the x-component of the filtration velocity and the corresponding Reynolds number.

In the third steady-laminar case, regime (c), recirculation zones are formed in the wake behind struts. The flow is still steady and laminar. Permeability starts to drop significantly, again implying that the strain rate near the solid-fluid interface increases faster than the filtration velocity. This can be understood by recognizing that the regions containing the recirculation zones have a very limited contribution to the mass flow rate through the foam volume. On the other hand, the mass flow rate is increased compared to previous flow regime (b). As the majority of the increased mass flow rate has to pass through a decreased volume, the inertial core tightens. This results in a larger increase of the strain rate near the solid-fluid interface than of the filtration velocity. The same reasoning can be made

for flow regime (d), where the flow becomes unsteady. This seems to occur at Re≈30, which is in accordance with Magnico et al. [20] who found 31.5. The region with limited mass flow rate, in the wakes downstream the struts, further increases due to the unsteadiness. This can be observed by comparing the details of flow regimes (c) and (d) in Figure 6. Another consequence is that the inertial core in the centre of the pores further narrows. Increasing the Reynolds number above a certain value (Re>115 in this case) results in an equilibrium between the increment of filtration velocity and strain rate. This is characterised by highly unsteady flow, where local turbulent spots start to appear. Note, however, that the viscous boundary layer still is laminar. It is unclear when this also becomes turbulent.

Inertial factor

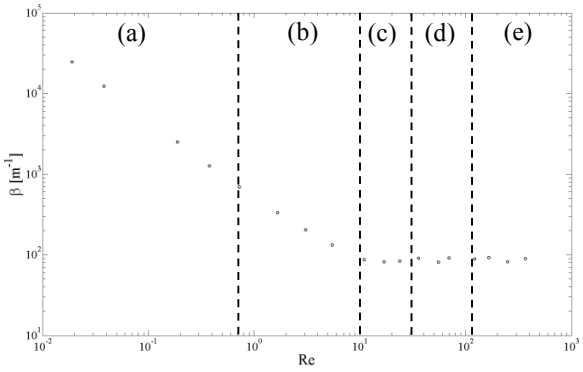

Figure 7 Inertial loss factor as a function of Reynolds number. The five flow regimes, as given in Figure 5, are indicated.

The inertial loss factor, based on the definition given by equation (6), is shown in Figure 7. The nearly constant value, for Re>10 is $\beta = 86.7$ m^{-1}. The experimental research of Dukhan et al. [6] yielded 89.5. The difference might be contributed to small deviations between the foam geometry used in their paper and the numerical representation used here. To give a conclusive answer, a sensitivity study needs to be done. This is out of the scope of this paper and will not be discussed.

Looking at equation (6), the inertial loss factor is defined as the ratio of the intrinsically volume averaged pressure force to the kinetic energy of the fluid. This pressure force is determined by the pressure distribution over the surface area of the solid-fluid interface. Upstream a strut, there is a stagnation zone where kinetic energy reduces to zero and results in a region with high pressure. Downstream, a distinction has to be made between flow regimes with or without recirculation regions in the wakes behind struts. In case of no recirculation (Re<10), the inertial loss factor decreases with increasing Reynolds number. This means that the pressure force increases at a lower rate than the averaged kinetic energy in the flow domain. From the moment that the recirculation regions in the wakes downstream the struts appear (Re>10), the increment of pressure force and averaged kinetic energy is equal. This is characterised by a nearly constant inertial loss factor.

For flow regime (a), Re<0.7, known as the Darcy regime [20], it is surprising to find an increasing inertial loss factor when Re decreases because in this regime, the Forchheimer extension (i.e. second term in equation (1)) is expected to vanish. With the definition of the inertial loss factor, given by equation (6), this is not the case. Examining the ratio of the Darcy term to the total pressure drop reveals a constant value of 0.32, for Re<0.7. For higher Reynolds numbers it decreases significantly and was 0.02 for the highest Reynolds number studied in this paper (Re=370). This suggests that the pure Darcy regime is not reached for the studied structure; at least not for the studied Reynolds numbers and with the used definitions of the flow properties. A closer inspection of the pressure distribution on the solid-fluid interface shows indeed a significant variation, even for the lowest Reynolds numbers. Therefore, based on physical grounds, the Forchheimer extension is needed for the studied range of Reynolds numbers, to be able to reconstruct the applied pressure drop gradient within 1.2% accuracy. As mentioned earlier, Dukhan et al. [6] assumed that the Forchheimer extension is negligible in the Darcy regime, which might explain the difference in permeability between their experimental and our numerical results. It seems that the pressure forces which act on the solid-fluid interface are contributed to the Darcy term.

Pressure drop graph

It is interesting to examine the pressure drop data in a classical way, i.e., plotting pressure gradient versus velocity and fitting a second order polynomial through the data. The obtained equation is compared with equation (1), from which both flow properties can be derived. The permeability and inertial loss factor are respectively $3.8\text{x}10^{-7}$ m² and 85.9 m^{-1}, which is in agreement with the numbers obtained by applying first principles, for the unsteady flow regimes.

As indicated by Innocentini et al. [3], the amount of data has a severe impact on the derived flow properties. Therefore, flow properties are derived per five consecutive data points. This indeed shows that for the low Reynolds number cases, the Forchheimer contribution reduces to less than 2% and indicates that only the first term of equation (1) (i.e. the Darcy term) is needed to reconstruct the applied pressure drop gradient. The permeability is $4.2\text{x}10^{-7}$, which is one third of the number obtained via a first-principles analysis. As indicated earlier, deriving the flow properties by fitting a second-order polynomial to pressure drop data, makes no clear distinction between viscous and pressure forces. The pressure drop reconstruction via the fitting method shows a maximum deviation of ±15% over the complete range of Reynolds numbers.

CONCLUSION

A method based on first principles is proposed to close the volume-averaged Navier-Stokes equations in the case of incompressible flow with a Newtonian fluid. The terms which describe the microscopic flow physics on a macroscopic scale take the volume-averaged viscous- and pressure forces in account. Both forces are source terms on the macroscopic

momentum balance. These forces are respectively related to permeability and inertial loss factor, giving both parameters a clear physical meaning.

Careful numerical simulations allows to compute both forces. This is done for one foam structure and for a Reynolds number ranging from 0.019 to 370. This covers five flow regimes: (a) steady laminar with limited inertial core, (b) steady laminar with inertial core spanning a foam-cell, (c) steady laminar with recirculation zones in the wakes downstream the struts, (d) unsteady laminar with periodic vortex shedding and (e) highly unsteady with chaotic flow structures. Permeability shows a great dependency on the flow regimes. The inertial loss factor becomes constant when recirculation regions appear in the wakes behind the struts.

In the flow regimes without recirculation behind the struts, i.e. regimes (a) and (b), the inertial loss factor increases with decreasing Reynolds number. Based on the first-principle analysis, it is found that in these flow regimes, the contribution of the viscous force on the total pressure drop remains constant at 0.32. In other words, the Forchheimer extension remains necessary to be able to reconstruct the applied pressure gradient. In case of the foam structure and flow regimes studied in this paper and the first-principles definition of the flow parameters, it can be concluded that a pure Darcy regime in the classical sense is not valid. The pressure force contribution remains significant.

Analysing the same data with the often applied fitting of a second-order polynomial on the pressure drop/velocity data, does result in a negligible Forchheimer contribution in the Darcy regime. There is, however, no physical explanation for this; rather, it seems to be a result from the fitting procedure. It should be noted that the authors do not question the validity of the Darcy law, because it depends on many factors, such as the definition of the flow properties and the porosity of the studied porous medium.

ACKNOWLEDGEMENTS

The authors want to express gratitude to Bekaert for the close cooperation and financial support. The institute for the Promotion of Innovation by Science and Technology (IWT Vlaanderen) is greatly acknowledged for their financial support.

REFERENCES

[1] Banhart, J., Manufacture, characterisation and application of cellular metals and metal foams, *Progress in Material* Science, Vol. 46, 2001, pp. 559-632

[2] Bonnet, J.P., Topin, F., Tadrist, L., Flow laws in metal foams: compressibility and pore size effects, *Transport in Porous* Media, Vol. 73, 2008, pp. 233-254

[3] Innocentini, M.D.M., Salvini, V.R., Pandolfelli, V.C., Coury, J.R., Assessment of Forchheimer's equation to predict permeability of ceramic foams, *Journal of the American Ceramic Society*, Vol. 7, 1999, pp. 1945-1948

[4] Dukhan, N., Ali, M., Effect of confining wall on properties of gas flow through metal foam: an experimental study, *Transport in Porous Media*, Vol. 91, 2012, pp. 225-237

[5] Dukhan, N., Patel, K., Effect of sample's length on flow properties of open-cell metal foam and pressure-drop correlations, *Journal of Porous Materials*, Vol. 18, 2011, pp. 655-665

[6] Dukhan, N., Minjeur, C.A., A two-permeability approach for assessing flow properties in metal foam, *Journal of Porous Materials*, Vol. 18, 2011, pp. 417-424

[7] Bear, J., Dynamics of fluids in porous media, *American Elsevier Publishing Company, Inc.*, 1988

[8] Cushman, J.H., Bennethum, L.S., Hu, B.X., A primer on upscaling tools for porous media, *Advances in Water Resources*, Vol. 25, 2002, pp. 1043-1067

[9] Whitaker, S., The method of volume averaging, *Kluwer Academic Publishers*, 1999

[10] Gray, W.G., A derivation of the equations for multiphase transport, *Chemical Engineering Science*, Vol. 30, 1975, pp. 229-233

[11] Whitaker, S., The Forchheimer equation: a theoretical development, *Transport in Porous Media*, Vol. 25, 1996, pp. 27-61

[12] Brun, E., Vicente, J., Topin, F., Occelli, R., Clifton, M.J., Microstructure and transport properties of cellular materials: representative volume element, *Advanced Engineering Materials*, Vol. 11, 2009, pp. 805-810

[13] De Jaeger, P., T'Joen, C., Huisseune, H., Ameel, B., De Paepe, M., An experimentally validated and parameterized periodic unit-cell reconstruction of open-cell foams, Vol. 109, 2011, pp. 1-11

[14] Versteeg, H.K., Malalasekera, W., An introduction to computational fluid dynamics, *Pearson Education Limited*, 2007, pp. 108

[15] Hutter, C., Allemann, C., Kuhn, S., Rudolf von Rohr, P., Scalar transport in a milli-scale metal foam reactor, *Chemical Engineering Science*, Vol. 65, 2010, pp. 3169-3178

[16] De, A.K., Dalal, A., Numerical simulation of unconfined flow past a triangular cylinder, *International Journal for Numerical Methods in Fluids*, Vol. 52, 2006, pp. 801-821

[17] Onstad, A.J., Elkins, C.J., Medina, F., Wicker, R.B., Eaton, J.K., Full-field measurements of flow though a scaled metal foam replica, *Experimental Fluids*, Vol. 50, 2011, pp. 1571-1585

[18] Pope, S.B., Turbulent flows, *Cambridge University Press*, 2003

[19] Davidson, L., Large Eddy Simulation: how to evaluate resolution, *International Journal of Heat and Fluid Flow*, Vol. 30, 2009, pp. 1016-1025

[20] Magnico, P., Analysis of permeability and effective viscosity by CFD on isotropic and anisotropic metallic foams, *Chemical Engineering Science*, Vol. 64, 2009, 3564-3575